Solvothermal synthesized boron doped TiO$_2$ catalysts: Photocatalytic degradation of endocrine disrupting compounds and pharmaceuticals under visible light irradiation

Esra Bilgin Simsek

Yalova University, Chemical and Process Engineering Department, 77100, Yalova, Turkey

ABSTRACT

Boron doped TiO$_2$ (B-TiO$_2$) photocatalysts with visible light activity were successfully synthesized by solvothermal method. The characterizations of the synthesized products were carried out by XRD, SEM-EDAX, BET, XPS, TGA-DTG and UV–vis spectroscopy. The band gap values of TiO$_2$ were decreased with the increase of the boron doping level. XPS analysis revealed that the interstitial TiO$_2$ structure was modified via formation of Ti—O—B bonds. Photocatalytic degradations of endocrine disrupting compounds (2,4-dichlorophenol (DCP), bisphenol-A (BPA)) and non-steroidal anti-inflammatory drugs (ibuprofen (IBU), flurbiprofen (FLU)) were examined by using raw and boron doped TiO$_2$ catalysts under UV-A and visible irradiation. Boron doping can remarkably enhance light utilization and improve the photocatalytic activity of TiO$_2$ toward the selected organics. The effects of boron content, initial solution pH and H$_2$O$_2$ on the photocatalytic performance were studied. The BPA, DCP, IBU and FLU reaction rate constants of B-TiO$_2$ (8 wt.% B) were found as k$_{BPA}$ = 5.989 × 10^{-2}, k$_{DCP}$ = 2.087 × 10^{-2}, k$_{IBU}$ = 1.818 × 10^{-2}, and k$_{FLU}$ = 1.319 × 10^{-2} min^{-1}. B-doped TiO$_2$ catalysts were found to be effective for the consecutive degradation tests referring their potentiality in extended applications.

© 2016 Elsevier B.V. All rights reserved.

1. Introduction

In the last decades, all over the world, attention has been paid to the elimination of endocrine-disrupting compounds (EDCs) and pharmaceutically active compounds (PhACs) detected in water bodies and wastewater effluents [1]. The occurrence of EDCs in the water supplies influences the aquatic lives and other life-forms through consumption of contaminated water [2]. Bisphenol A (BPA) and chlorophenols (CPs) which are commonly found in wastewater, pose serious risks to the environment since they were noticed as inducing an endocrine disruption effect. BPA is widely used as an intermediate in the production of polycarbonate plastics and epoxy resins and it finds its way in the aquatic environment via degradation of several BPA containing materials [2–4]. BPA concentration can be as high as 17.2 mg/L at the site of industrial effluents and in leachates from landfills containing compost materials, liquid manures and waste plastics [2]. 2,4-dichlorophenol (DCP) as one of typical phenolic substances, is used as a biocide, wood treatment agent, and as a by-product of bleaching in paper mills [5]. In several countries DCP concentrations in the surface waters were
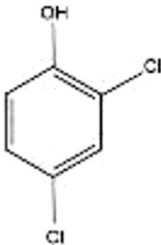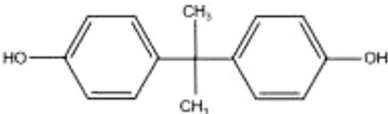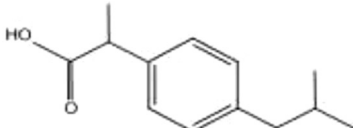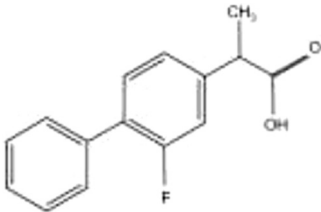
reported as in the range of <1 to 20 µg L^{-1} [5]. Due their widely usage and biodegradability, among EDCs, BPA and DCP were chosen as the model substrates to examine the photocatalytic activities of the synthesized catalysts. On the other hand, non-steroidal anti-inflammatory drugs (NSAIDs) are a class of drugs with analgesic and antipyretic and anti-inflammatory effects in higher doses [6]. Ibuprofen (IBU) and flurbiprofen (FLU)—as the members of NSAID group– were chosen for the current study as they are the most consumed medicines.

Advanced oxidation processes (AOPs) have been extensively employed due to their effectiveness in degradation reactions especially for hazardous pollutants [7]. Heterogeneous photocatalysis, one of the AOPs, is an effective technique for the degradation of persistent organic compounds. Due to its strong oxidizing power, long-term photo-chemical corrosive resistance and nontoxicity, titanium oxide (TiO$_2$), especially its anatase phase, is a well-known efficient semiconductor for its extensive application in degradation of several organic pollutants in both gaseous and liquid phases [8].

Besides post separation difficulties related with the powder form of TiO$_2$, it could only use <5% solar energy for photodegradation due to its large band gap energy (3.2 eV) which restricts its application [9]. Hence, many researches have focused on how to develop its photocatalytic activity from UV into the visible light

E-mail addresses: esrabilgin622@gmail.com, ebilgin.simsek@yalova.edu.tr

Table 1
Molecular structures and pK_a values of target compounds .

Compound	Molecular Formula	Structure	pK_a
2,4-Dichlorophenol	$C_6H_3Cl_2OH$		7.85
Bisphenol-A	$C_{15}H_{16}O_2$		10.3
Ibuprofen	$C_{13}H_{18}O_2$		4.9
Flurbiprofen	$C_{15}H_{13}FO_2$		4.22–4.27

range to enable the utilization efficiency of solar energy [10]. Metals and non-metals ions incorporation is a promising method as it favors the electron–hole separation and enhances the visible light absorption property [11]. Boron as a dopant have recently drawn special attention as the photoactivity increased efficiently under visible light [8,12–18]. Quiñones et al. [13] reported that B-doped TiO_2 has the potential application for four recalcitrant pesticides (diuron, o-phenylphenol, MCPA and terbuthylazine) under simulated solar irradiation and they obtained that the B-doped catalyst was stable and maintained 75% mineralization after three cycles. Wu et al. [12] have found that carbon and boron co-doped TiO_2 photocatalyst have synergistic effect for the effective photodegradation of DCP under visible light irradiation. Zheng et al. [17] synthesized boron doped titanium oxide hybrid microspheres by hydrothermal method for the methylene blue degradation under simulated sunlight. They clarified that boron doping improved crystallinity of anatase titania and increased the amount of superficial hydroxyl groups. Cavalcante et al. [18] evaluated B-doped TiO_2 in the photodegradation of metoprolol which is a β-blocker among pharmaceuticals. They reported that 5% (w/w) B-doped TiO_2 exhibited greater efficiency (70% removal) than pure TiO_2 (48% removal).

To the best of our knowledge and according to the literature search, the photocatalytic degradation of BPA, IBU and FLU over B doped TiO_2 under UV-A and visible-light irradiation has been investigated for the first time in this study. Visible light activated B-TiO_2 catalysts were utilized for the degradation of endocrine disrupting compounds (DCP, BPA) and non-steroidal anti-inflammatory drugs (IBU, FLU) in aqueous solutions. TiO_2 and B-TiO_2 catalysts were characterized by XRD, XPS, FTIR, SEM-EDX, BET, TGA-DTG and UV–vis absorbance spectroscopy.

2. Materials and methods

2.1. Chemicals and reagents

All chemicals were obtained commercially and used without further purification. 2,4-dichlorophenol (DCP), bisphenol-A (BPA), ibuprofen (IBU) and Flurbiprofen (FLU) were purchased from Sigma–Aldrich. The molecular structures and properties of the chemicals used as pollutants were given in Table 1.

2.2. Catalysts preparation

The synthesis of TiO_2 and B-doped TiO_2 catalysts was carried out following a modified solvo-thermal procedure previously reported [12]. Initially, 12 mL tetrabutyl titanate (Sigma–Aldrich, 97%) was dissolved into 24 mL anhydrous ethanol (solution A). Secondly, 20 mL ethanol and desired amount of boric acid (Sigma, Aldrich) were mixed in a beaker, then PEG-600 was added to the mixture, adjusting the pH with concentrated nitric acid (68% wt.) to prepare solution B. After solution A was dropwisely added into solution B under magnetic stirring. The resulting sol was stirred for 2 h and the gel was aged for 4 days. Then, the gel was operated by hydrothermal treatment in a Teflon-lined stainless steel autoclave at 180 °C for 10 h. The products were cooled at room temperature, washed with de-ionized water and ethanol, dried and calcined at 500 °C for 3 h. B-doped TiO_2 catalysts were prepared with weight content of boron: 1.0, 3.0, 5.0 and 8.0 wt.% in order to examine the effect of the introduction of boron species both in the structural and in the photocatalytic properties of catalyst. For comparison, raw TiO_2 catalyst was synthesized by the same method only without addition of H_3BO_3.
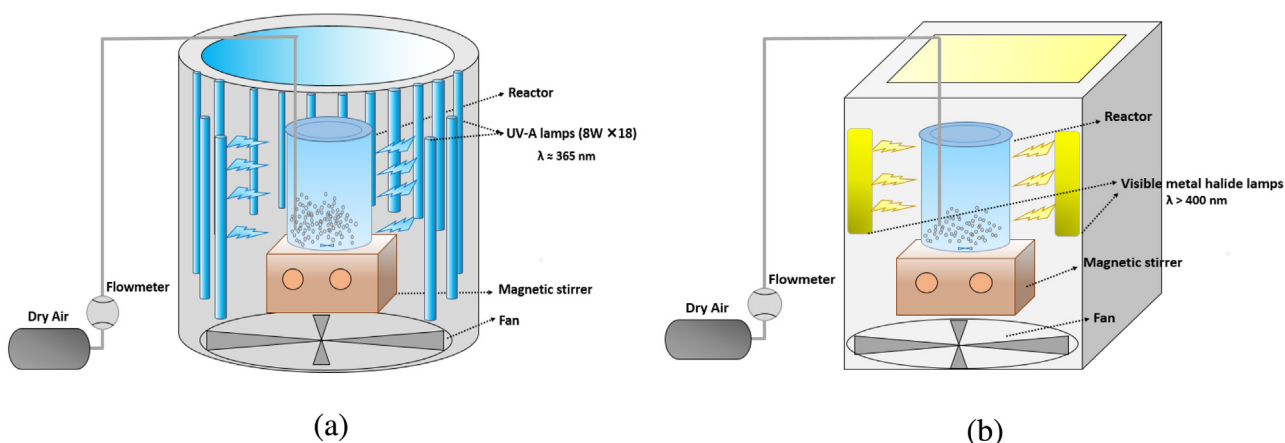
Fig. 1. Schematic representation of UV-A light (a) and (b)Visible light photoreactors.

2.3. Structural characterization

The crystal structure was analyzed by X-ray diffractometer (XRD, 600 SHIMADZU, CuKα). The Fourier transfer infrared (FTIR) spectrum was recorded by Perkin Elmer Spectrum One using attenuated total reflectance method, in the wave number range of 600–4000 cm^{-1}. Thermogravimetric analysis (TG–DTG) of raw and B-doped TiO$_2$ catalysts was carried out in air flow with a Simultaneous TGA–DTA Instrument (SEIKO) in the range 20–1000 °C at 10 °C min^{-1} heating rate. The surface area, total pore volume and pore size distribution were measured by nitrogen adsorption/desorption at 77 K using QuadraSorb Station 2 instrument. The surface areas were calculated by the Brunauer–Emmett–Teller (BET) method, and the pore size distribution and total volume were determined by the Brunauer–Joyner–Hallenda (BJH) method. Potentiometric titration data were obtained using a method described by Helfferich [19]. The morphology of catalysts was investigated by using scanning electron microscope (SEM) equipped with a Bruker energy dispersive X-Ray (EDX) detector (Philips XL30 ESEM-FEG/EDAX). In order to analyze B leaching, B-doped catalysts were washed with distilled water, samples were taken by time intervals and boron concentration was analyzed by with an atomic absorption spectrophotometer (Analytik Jena ContrAA 700 TR). Surface electronic states and functional groups were analyzed by X-ray photoelectron spectroscopy (Thermo Scientific K-Alpha X-ray Photoelectron Spectrometer). The ultraviolet–visible diffusion reflectance spectra (UV–vis DRS) of catalysts recorded with spectrophotometer (Perkin Elmer Lambda 35) using BaSO$_4$ as the reference standard in the wavelength range of 220–800 nm. The diffuse reflectance mode (R) was transformed to the Kubelka-Munk function F(R) to separate the extent of light absorption from scattering. The band gap values were calculated based on the modified Kubelka-Munk function [F(R)E$^{1/2}$] and the energy of the absorbed light (E) as follows in Eq. (1):

$$F(R)E^{1/2} = \left(\frac{(1-R)^2}{2R} \times h\upsilon \right)^{1/2} \qquad (1)$$

2.4. Reactor setup and photocatalytic degradation tests

UV-A light photocatalytic measurements were performed in a laboratory scale column-shaped stainless steel cabinet. Hexagonally placed 18 UV lamps (Philips TL 8 W Actinic BL, mainly emits 365 nm, Fig.S1) were used as UV-A light sources (Fig. 1a). Visible light irradiation experiments were performed in a square photoreactor (Fig. 1b) which consists of two visible metal halide lamps (Osram 150 W, λ: 400–800 nm, Fig.S2). The distance between the

lamp and the reactor was maintained at 10 cm. The system is cooled by ventilation through a fan installed at the bottom of the cabinet. Dry air is bubbled continuously through the reactor at a speed of 2 L min^{-1} in order to keep water solution saturated with oxygen and also to keep catalyst particles fluidization.

DCP, BPA, IBU and FLU are selected as simulated pollutants in order to evaluate the photocatalytic activities of TiO$_2$ and B-TiO$_2$ samples. For a typical experiment, 0.1 g of catalyst was dispersed in 100 mL of solution containing 20 mg L^{-1} initial concentration of each pollutant by ultrasonic bath for 10 min. In order to secure the establishment of adsorption/desorption equilibrium, prior to irradiation the catalysts with target pollutants were magnetically stirred in dark for 60 min. Before illumination, an aliquot of the equilibrated suspension was analyzed, being considered as the initial equilibrium concentration. After, UV-A or visible light sources were switched on. Aliquots of the suspension (4 mL) were periodically collected and filtered with syringe membrane filters (0.45 μm). The effects of solution pH (3.0, 6–6.5, 10.0), and effect of H$_2$O$_2$ (20 mM, 40 mM) on the photocatalytic degradation were investigated.

The durability tests of 8B-TiO$_2$ catalyst were carried out by using the same procedure as above and the product underwent four/five consecutive cycles, each lasting for 300–360 min. After each cycle, the catalyst was centrifuged, washed thoroughly with deionized water, and then added to fresh DCP, BPA, IBU and FLU solutions. In order to confirm the reproducibility of the results, the degradation experiments were carried out with duplicated runs for each condition, and the experimental error was calculated to be within ±5%.

2.5. Analytical method

All samples collected at time intervals were measured using a High Performance Liquid Chromatography (Dıonex Ultimate 3000 UHPLC) equipped with Acclaim C18 column (4,6 mm × 150 mm, 3 μm, 120 A^0). The wavelength of photodiode array detector (PDA) was 270 nm for BPA and 280 nm for DCP. For BPA analysis, the mobile phase was selected as acetonitrile and water (80/20; v/v) while methanol and water (70:30) was used as the mobile phase for DCP analysis at a flow rate of 0.2 mL min^{-1}.

The eluent used was acetonitrile/water (80/20, v/v) at a flow rate of 0.2 mL min^{-1} and the maximum adsorption wavelength (λ$_{max}$) was chosen as 214 nm for IBU and FLU analysis.

To investigate the mineralization of the pollutants, the total organic carbon (TOC) was analyzed using a Shimadzu 5000 TOC analyzer.
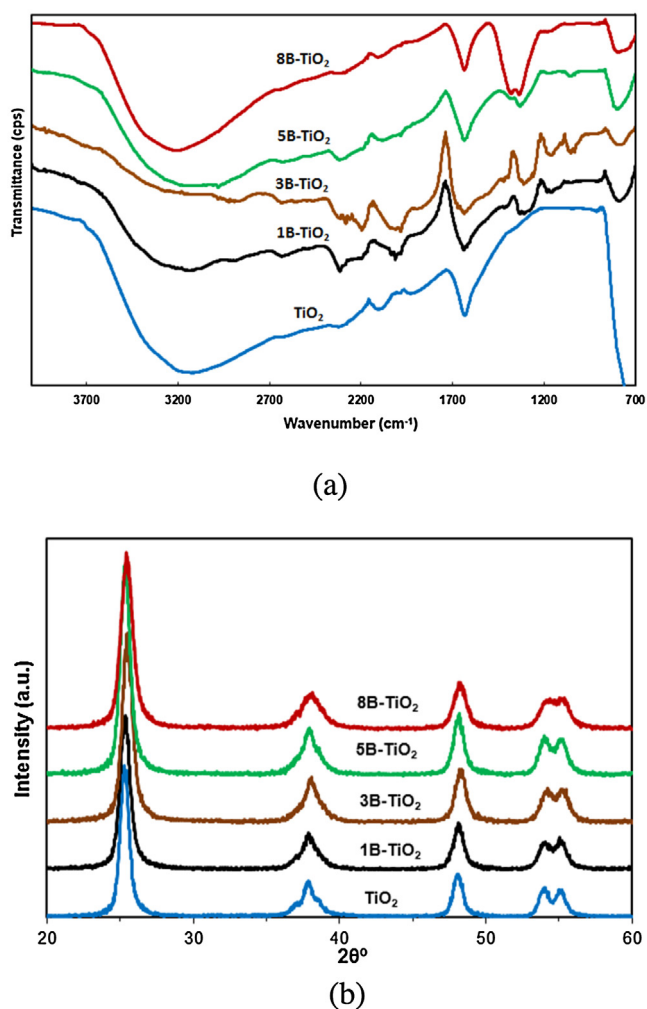
(a)

(b)

Fig. 2. FTIR spectra (a) and XRD patterns (b) pristine and boron doped TiO$_2$ catalysts.

3. Results and discussion

3.1. Catalysts characterization

The FTIR spectra of pristine and B doped titanium particles are shown in Fig. 2(a). The broad band in the 3400 and 1630 cm^{-1} range indicates surface adsorbed water and hydroxyl groups indicating of the presence of free hydroxyl groups of all catalysts. For pristine TiO$_2$ nanoparticles, the peaks below 700 cm^{-1} attributed to Ti—O—Ti vibrations [11,20]. After boron doping, new bands appear in the region 780–785 cm^{-1} indicating B—O vibrations in the unit BO$_3$. [21]. Peak et al. [22] stated that the peaks for tetrahedral boron as trigonal B—O stretching, B—O—H bending, and tetrahedral B—O stretching appear in the 700–1000 cm^{-1} region. They reported that boric acid species namely polymeric trigonal boron, aqueous boric acid and outer-sphere boric acid are potential sources of the peak around 1300 cm^{-1}. Therefore, due to the doping of boron atoms, the increased intensity in the peaks at 1331 cm^{-1} (for 5B-TiO$_2$) and 1335 cm^{-1} (for 8B-TiO$_2$) could be ascribed to the asymmetric B—O stretching on the surface. Also, the peaks at 1146–1165 cm^{-1} belong to B—O bonds in the B$_2$O$_3$ crystal. Liang et al. [15] emphasized that the peaks around 1393 cm^{-1} might be attributed to the Ti—O—B bond.

The XRD patterns (Fig. 2(b)) of the both raw TiO$_2$ and B/TiO$_2$ photocatalysts are of well-developed anatase phase with characteristic peaks at 25.42°, 38.06°, 48.24°, 54.62° and 55.58°. No peak

positions of brookite or rutile TiO$_2$ was found in the patterns. The diffraction peaks for boron containing phases were not observed indicating boron doping did not affect the crystal phase structure of catalysts which is in agreement with the findings from previous studies [18,24]. Therefore, it can be concluded that boron has highly dispersed on TiO$_2$ and solvothermal method is favorable in synthesizing doped-fine particles of high crystallinity of anatase phase.

The curves of thermogravimetry (TG) and differential thermogravimetry analysis (DTG) of TiO$_2$ and 8B-TiO$_2$ photocatalysts are shown in Fig. 3(a). The TGA curve of TiO$_2$ and 8B-TiO$_2$ catalysts reveal negligible weight losses of 2.0–2.9% below 150 °C likely attributed to the evaporation of water and other volatile organics. The subsequent weight loss of 0.9% happened within 300–600 °C, and the large portion of the remaining sample, which corresponds to 96–97% of the original sample weight is observed stable at 600 °C and above due to the inorganic content (i.e. TiO$_2$).

Specific surface area of TiO$_2$ based catalysts was measured as a function of boron loading. The textural properties of TiO$_2$ and B/TiO$_2$ catalysts are listed in Table 2. Compared to raw TiO$_2$ (64.62 m^2/g), the surface area of the doped catalysts increased with increasing B content (83.23 m^2/g for 1B-TiO$_2$ and 90.91 m^2/g for 5B-TiO$_2$). However, the BET surface area of 8B-TiO$_2$ sample decreases slightly to 90.24 m^2/g and its pore volume drops to 0.185 cm^3/g, indicating that increased boron amount could result in the aggregation of the particles. Similar phenomena were observed by other researchers [8,12].

Fig. 3(b) shows the pore size distribution curves TiO$_2$ and B-TiO$_2$ samples. It reveals that the pore size regions of catalysts are mainly in the range from 3 nm to 14 nm. For TiO$_2$ sample, the region possess two sharp maximums at about 4.7 and 8.9 nm while it decreased to 3.80–4.4 nm region for 1B-TiO$_2$ and 3B-TiO$_2$ samples. Further increase in boron content leads to higher pore diameter as was observed for 5B-TiO$_2$ (7.78 nm) and 8B-TiO$_2$ (10.64 nm) which could be related with the aggregation of particles resulting formation of mesopores with increasing amount of boron.

UV–vis diffuse reflectance spectra of the catalysts are shown in Fig. 4. It can be seen that pure TiO$_2$ had no absorption in the visible light region (>400 nm), while 5B-TiO$_2$ and 8B-TiO$_2$ catalysts displayed a weak absorption band in the range of 400–600 nm. Table 2 shows the band gap energy according to Tauc's expression from the UV–DRS spectra. The E$_g$ values of catalysts were found decreasing with increasing boron content. This could be attributed to the presence of oxygen vacancies, which is responsible for the red shifted optical absorption [12]. Similar phenomenon was observed by Wu et al. [12] while different trend was found by other researchers [13,16]. They reported that the E$_g$ value decreased with increasing boron content from 0.5 to 10 wt.% ascribing to the low mixing of 2p boron bands with 2p oxygen bands.

In order not to excess the B limit in drinking water regulated as 1 mg/L by European Union standards [13], boron content was determined by time intervals in aqueous media and the data is shown in Fig. 5. The B concentration in solution reached maximum values as 0.25, 0.35, 0.51 and 0.61 mg/L for 1B-TiO$_2$, 3B-TiO$_2$, 5B-TiO$_2$ and 8B-TiO$_2$, respectively. On the other hand, the point of zero charge (PZC) values which the net surface charge is zero were determined for the catalyst. The pH$_{PZC}$ for both raw and boron doped TiO$_2$ samples found in the range of 6.4–6.8 indicating the boron content did not significantly change the surface charge.

Fig. 6 shows the SEM micrographs obtained for the pristine and boron doped TiO$_2$ samples. As can be seen, boron doping does not influence too far on the diameter and size distribution of TiO$_2$ materials, and the grains are homogeneous and round-shaped. The catalysts surface have dimensions in the range of 16–25 nm. The obtained amount in EDX analysis was approximately in good agreement with the boron doping contents. For 5B-TiO$_2$ and 8B-TiO$_2$, the
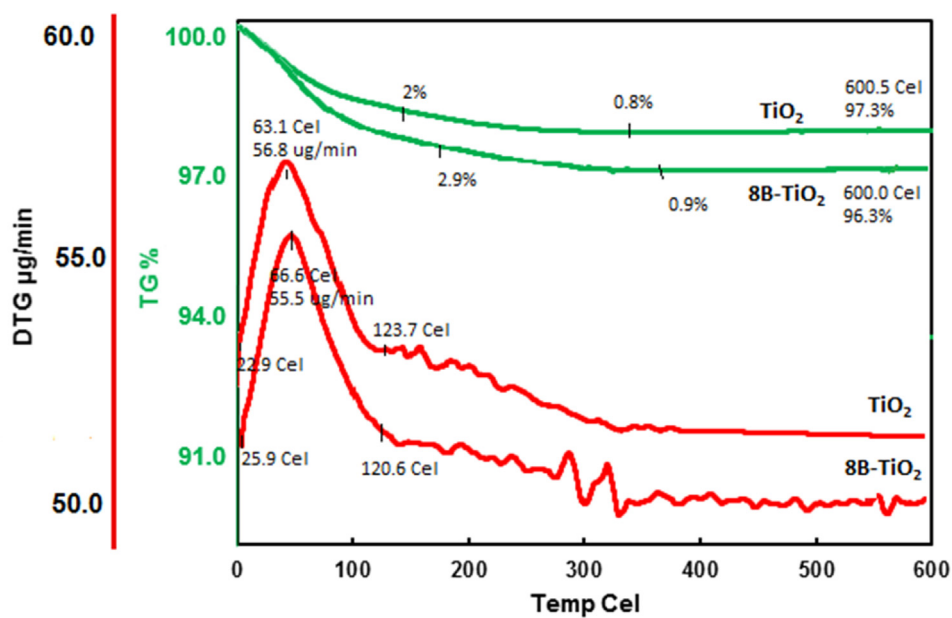
(a)
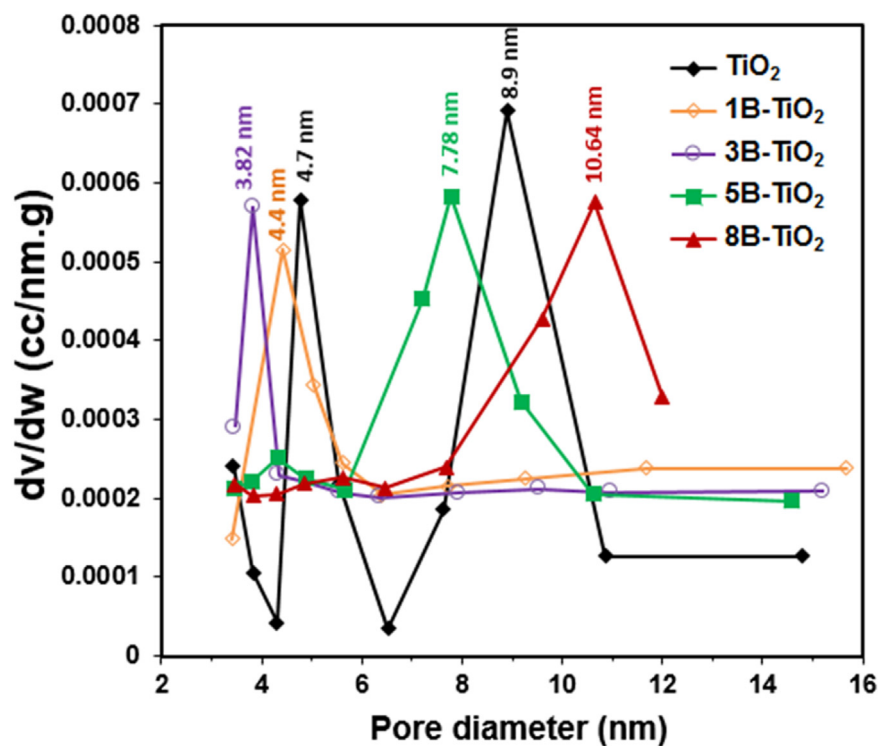
(b)

Fig. 3. TG/DTG profiles (a) and BJH pore size distribution (b) of catalysts.

Table 2
Properties of the catalysts.

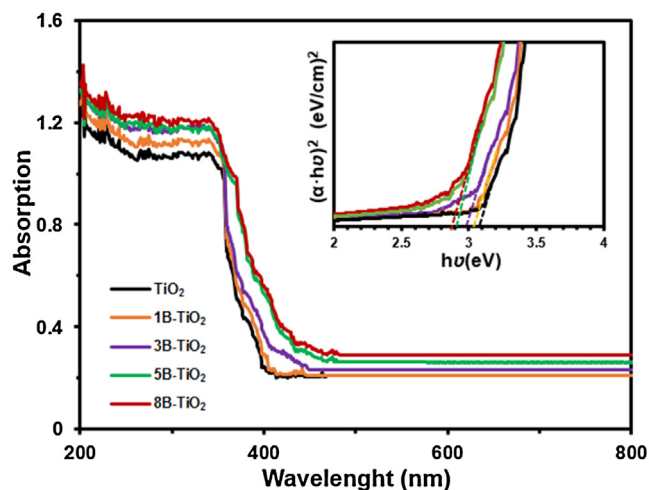| Sample	Specific surface Area, m²/g	Pore diameter (nm)	Pore volume, cm³/g	pH$_{PZC}$	Band gap energy, E$_g$ (eV)
TiO$_2$	64.61	9.10	0.120	6.4	3.09
1B–TiO$_2$	83.23	4.41	0.188	6.4	3.05
3B–TiO$_2$	85.78	3.82	0.191	6.4	3.00
5B–TiO$_2$	90.90	7.78	0.192	6.5	2.90
8B–TiO$_2$	90.23	10.64	0.185	6.8	2.89

Fig. 4. UV-vis diffuse reflectance spectra of catalysts. Inset shows the Kubelka-Munk transformed reflectance spectra.
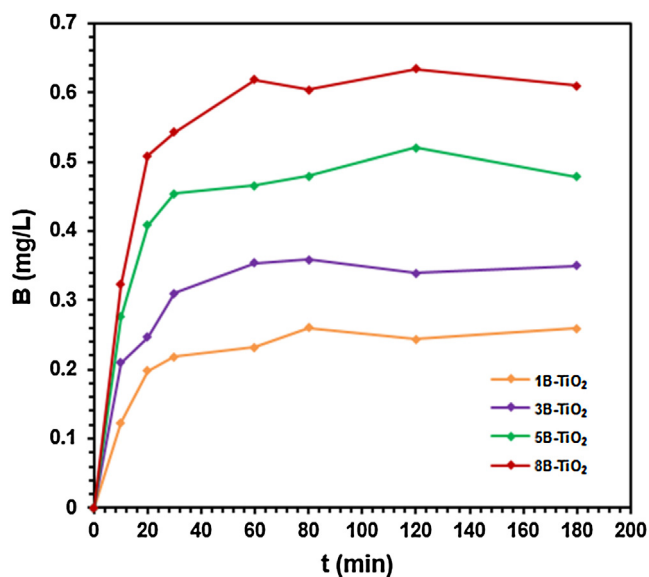

Fig. 5. B leaching of the B-TiO$_2$ samples during washing with H$_2$O (Catalyst dosage: 1 g/L).

boron contents were found as 6.85% and 8.63%, respectively. No impurities were obtained in the catalysts.

In order to examine the chemical compositions of raw and B-doped catalysts, X-ray photoelectron spectroscopy (XPS) was conducted with peak deconvolution. The wide XPS spectra (Fig. 7.) of TiO$_2$ catalysts show photo electron lines at a binding energy of about 563.08, 530.08, 459.08, 284.08, 59.08 and 39.08 eV, which can be attributed to Ti 2s, O 1s, Ti 2p, C 1s, Ti 3s and Ti 3p, respectively. The C element can be due to the residual carbon from precursor solution and the adventitious hydrocarbon from XPS instrument itself [23].

The Ti 2p spectra (Fig. 8.) showed two main peaks at 457.9 eV (52.9%) and 463.5 eV (25.0%) which could be defined as Ti 2p$_{3/2}$ and Ti 2p$_{1/2}$, respectively. After boron doping, the main peak has been shifted toward higher binding energy values (458.2 eV, 68.1%) due to the higher electronegativity of boron, thus confirming the formation of interstitial B in the form of Ti—O—B structures [13].

As shown in Fig. 9, O 1s peak of raw TiO$_2$ is composed of five chemical states. The first peak at 529.05 eV is related to oxygen in the Ti—O bond, and the second peak at 530.28 eV corresponds to

oxygen in the TiO$_2$ crystal lattice [24]. The O 1s region of 8B-TiO$_2$ is composed of four peaks at 529.68, 530.29, 531.11 and 532.2 eV. A new peak at 532.2 eV with atomic ratio of 7.79% appeared corresponding to B—O or Ti—O—B bonds, which is consistent with the result of XPS B 1s region. After B doping, the peaks at about 530 eV—ascribed to oxygen in TiO$_2$- decreased from 29% to 12% due to the formation of B—O bond. The intensity of peaks at 529.68 (Ti—O) and 531.11 eV (OH—) increased with boron doping. Zheng et al. [17] underlined the fact that the hydroxyl groups on the TiO$_2$ surface have favorable effect on the photocatalysis. As the hydroxyl group content (at 530 eV) on the surface of TiO$_2$ (5.6%) increased after the boron doping (8.0%) and as the general oxygen content of catalyst increased after doping (from 53.1% to 56.5%), it can be conclude that the boron incorporation resulted in enhancement of photo-catalytic efficiency of TiO$_2$.

The standard binding energy of B 1s (Fig. 10) in B$_2$O$_3$ or H$_3$BO$_3$ equals to 193.0 eV (B—O bond) and in titanium boride (TiB$_2$) equals to 187.5 eV (B—Ti bond). Artiglia et al. [25] stated that TiB$_2$ has a peculiar layered structure, whereas, in B$_2$O$_3$, interconnected BO$_3$ triangles are present, where B is at the center of a trigonal coordination. The B 1s signal presents a single peak centered at 191.79 which can be ascribed to Ti—O—B bond in the structure of 8B-TiO$_2$ catalyst [24,25]. Therefore, we can conclude that the boron is probably weaved into the interstitial TiO$_2$ structure, existing in the form of the Ti—O—B [24].

3.2. Photocatalytic activity measurements

Experiments were carried out with TiO$_2$ and B-TiO$_2$ samples under UV-A and visible light irradiation in order to compare the photocatalytic efficiencies towards DCP, BPA, IBU and FLU as degradation substrates. The selected compounds with concentration of 20 mg/L were illuminated with 1 g/L catalysts at pH ∼6–6.5. Photodegradation kinetics for both UV-A and visible light are shown in Fig. 11.

In the first step, the photocatalytic activities of catalysts were investigated under UV-A light irradiation. For comparison, under UV-A irradiation over a period of 300 min, no self-conversion of the selected pollutants was obtained in the absence of photocatalyst, referring that the direct photolysis could not significantly degrade the selected pollutants. As shown in Fig. 11, after 4 h of UV-A light irradiation by TiO$_2$ and 8B-TiO$_2$ catalysts, about 75.7% and 89.7% of DCP was diminished; while that of for BPA was calculated as 97.3% and 99.1%, respectively. In addition, when 8B-TiO$_2$ catalyst was used in UV-A light reaction, the degradation efficiencies of IBU (89.1% for TiO$_2$; 96% for 8B-TiO$_2$) and FLU (93% for TiO$_2$; 98% for 8B-TiO$_2$) increased slightly compared with TiO$_2$. In general for all pollutants, 1B-TiO$_2$ catalyst showed similar performance with pure TiO$_2$ while 5B-TiO$_2$ and 8B-TiO$_2$ were found as better efficient catalysts under UV-A irradiation.

Under visible light illumination, TiO$_2$ exhibited lower degradation for DCP (20.2%) and BPA (46.0%) after 300 min of treatment, while higher BPA (97.7%, 4 h) and DCP (75.1%, 5 h) removals were achieved using 8B-TiO$_2$ catalyst. Similar behavior was obtained for IBU and FLU, 81–85% degradation (5 h) was obtained with 8B-TiO$_2$ catalyst while nearly 40% achieved with raw TiO$_2$. In general, 1B-TiO$_2$ catalyst showed similar performance with pure TiO$_2$ and was found less effective in visible illumination among B-TiO$_2$ catalysts. The photocatalytic performances were found in the order of 8B-TiO$_2$ > 5B-TiO$_2$ > 3B-TiO$_2$ > 1B-TiO$_2$ ≈ TiO$_2$ and 8B-TiO$_2$ was chosen for further investigation.

Liang et al. [15] stated that several factors may enhance the catalytic performance of B–doped TiO$_2$. They underlined that B–doped TiO$_2$ forms new chemical bonds B—O—Ti and B—O—B in interstitial positions, which benefit photodegradation. In addition, Fu et al. [27] suggested that the doped B atoms might act as electron traps and
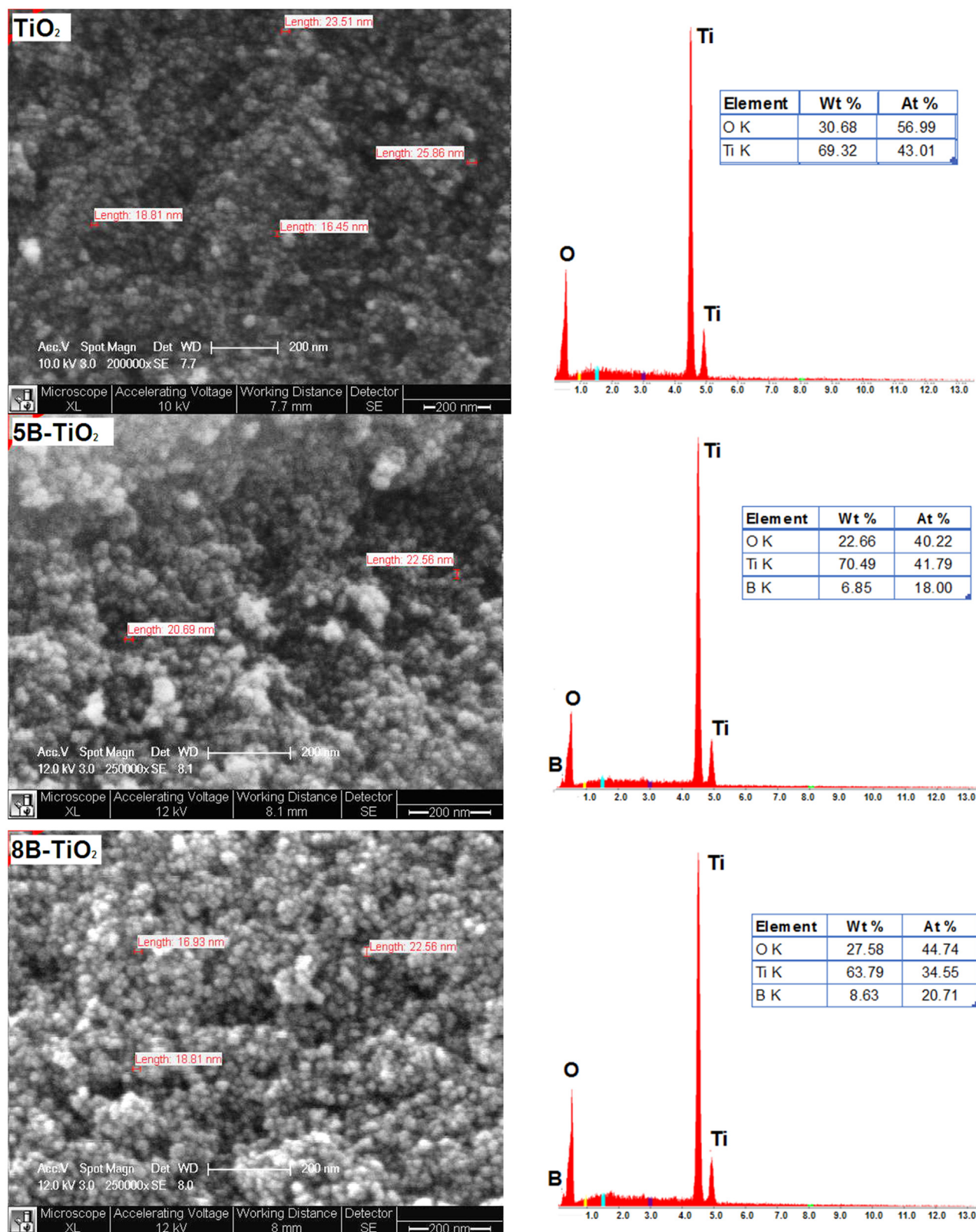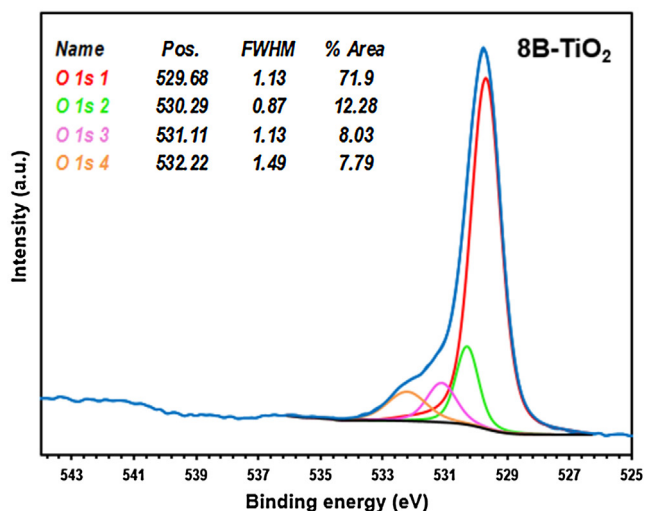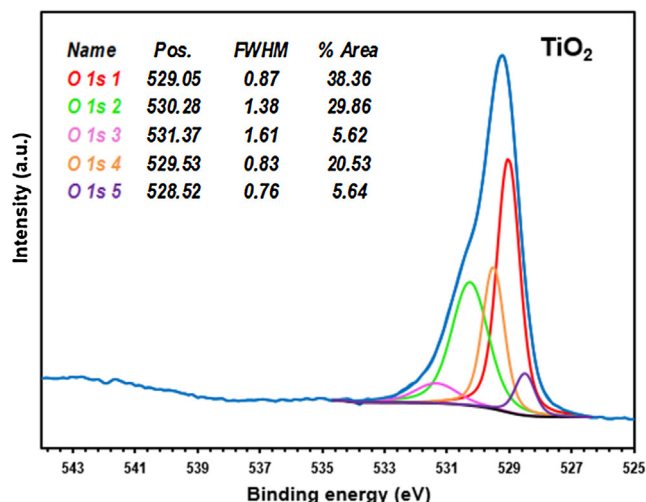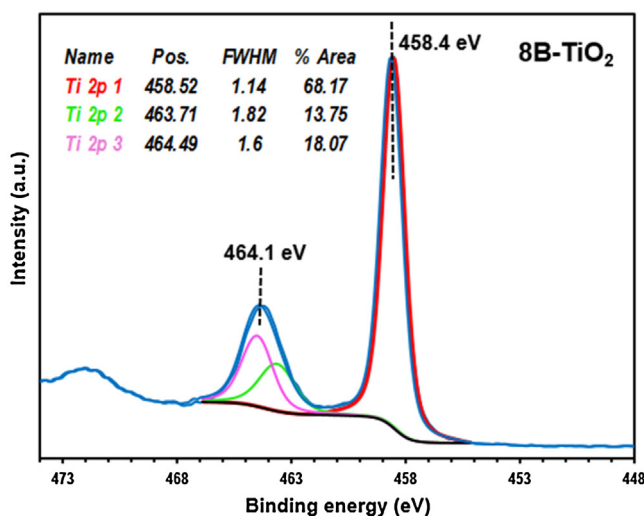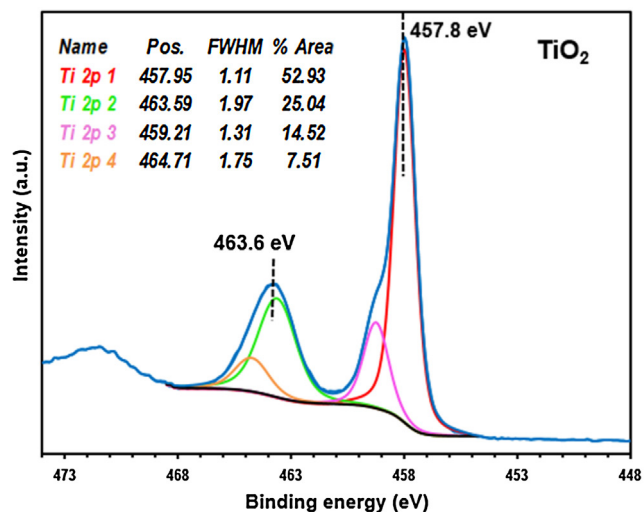
Fig. 6. SEM and EDX analysis of TiO_2, 5B-TiO_2 and 8B-TiO_2 catalysts.

facilitate the separation of photogenerated electron–hole pairs due to its electron deficient and oxytropic characteristics. In the current work, the modification on the radiation absorption properties regarding the decrease in the forbidden band gap plays the most important role in the behavior of the TiO_2 and B-TiO_2 catalysts.

It is well known that the photocatalytic degradation rate generally fits with the *Langmuir–Hinshlwood* kinetic model:

$$r = k_r \theta = -\frac{dC}{dt} = k_r \frac{K_a C}{1 + K_a C} \tag{2}$$
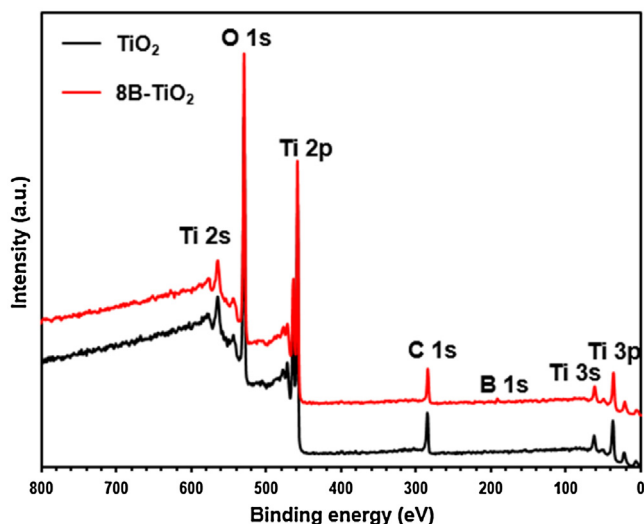
Fig. 7. XPS survey scan TiO_2 and 8B-TiO_2 catalysts.

Fig. 8. Deconvolution of Ti 2p core levels of TiO_2 and 8B-TiO_2 catalysts.

Fig. 9. Deconvolution of O 1 s core levels of TiO_2 and 8B-TiO_2 catalysts.

where r is the rate of degradation, K_a represents adsorption constant and k_r reflects the true rate constant including parameters such as the coverage in oxygen, the catalyst loading, the flux of efficient photons, etc. At low initial concentrations, the term K_aC in the denominator can be neglected with respect to unity and the rate becomes, apparently, first order:

$$r = -\frac{dC}{dt} = k_r K_a t = k_{app} t \tag{3}$$

The equation can be simplified as:

$$\ln\left(\frac{C}{C_0}\right) = -k_{app} t \tag{4}$$

Where k_{app} (min^{-1}) is the apparent constant of pseudo-first-order. The calculated rate constants (k_{app}) under UV-A and visible light irradiation were listed in Table 3. As can be seen on both Fig. 11 and Table 3, the photocatalytic activity is highly dependent on the light source where k_{app} constants calculated under UV-A light irradiation were found much higher than that of visible light. Considering the fact that the photon energy is lower in visible light [26], the degree of light absorption by the catalyst surface is significantly reduced resulting lower kinetic constant. Moreover, the photocatalytic efficiency is also related with the dopant amount of boron where k_{app} values increased with increasing boron content. The apparent rate constants are calculated as $k_{BPA} = 5.989 \times 10^{-2}$, $k_{DCP} = 2.087 \times 10^{-2}$,

Table 3
The apparent kinetic constants k_{app} and R^2 values of TiO_2 and $B-TiO_2$ catalysts [pH ~6–6.5, T = 25–30 °C, C_0 = 20 mg L^{-1}, Catalyst dosage = 1 g L^{-1}, Q_{air} = 2 L min^{-1}].

Process	DCP		BPA		IBU		FLU	
	$k_{app} \times 10^{-2}$ (min^{-1})	R^2	$k_{app} \times 10^{-2}$ (min^{-1})	R^2	$k_{app} \times 10^{-2}$ (min^{-1})	R^2	$k_{app} \times 10^{-2}$ (min^{-1})	R^2
UV-A light irradiation								
TiO_2	2.457	0.956	4.040	0.993	3.368	0.941	2.271	0.986
$1B-TiO_2$	2.430	0.975	4.267	0.999	3.371	0.969	2.318	0.948
$3B-TiO_2$	2.475	0.969	5.454	0.959	3.374	0.950	2.361	0.971
$5B-TiO_2$	2.587	0.986	6.625	0.967	3.872	0.958	2.392	0.965
$8B-TiO_2$	2.603	0.949	6.692	0.959	3.890	0.987	2.560	0.983
Process	**DCP**		**BPA**		**IBU**		**FLU**	
	$k_{app} \times 10^{-2}$ (min^{-1})	R^2	$k_{app} \times 10^{-2}$ (min^{-1})	R^2	$k_{app} \times 10^{-2}$ (min^{-1})	R^2	$k_{app} \times 10^{-2}$ (min^{-1})	R^2
Visible light irradiation								
TiO_2	1.954	0.897	2.136	0.947	1.607	0.946	1.092	0.960
$1B-TiO_2$	1.821	0.996	2.457	0.931	2.120	0.977	1.183	0.976
$3B-TiO_2$	1.828	0.994	2.698	0.993	1.802	0.952	1.171	0.905
$5B-TiO_2$	2.079	0.988	4.552	0.980	1.831	0.944	1.309	0.959
$8B-TiO_2$	2.087	0.976	5.989	0.977	1.818	0.972	1.319	0.970
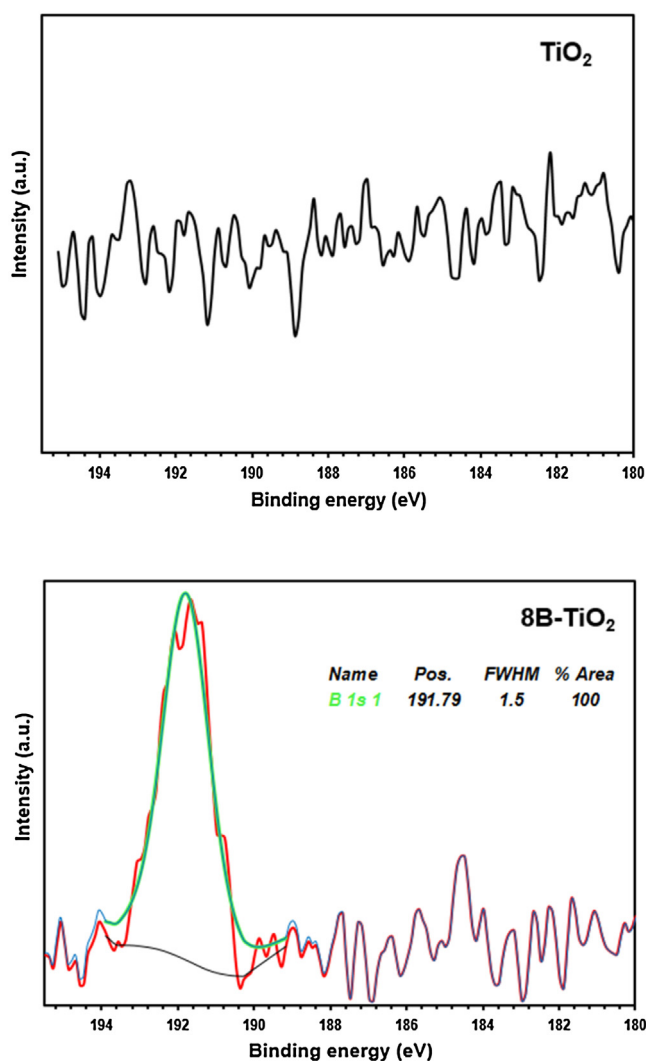
Fig. 10. B 1 s spectra of TiO_2 and $8B-TiO_2$ catalysts.

k_{IBU} = 1.818 × 10^{-2}, and k_{FLU} = 1.319 × 10^{-2} min^{-1}. Comparing the degradation efficiencies of $8B-TiO_2$ catalyst for 4 h illumination, the order of the reactivity was found to be BPA (97.7%) > IBU (79.4%) > FLU (71.0%) > DCP (66.6%). In photocatalytic oxidation reactions, when direct photolysis or adsorption have negligible

contributions, the main degradation occurs through hydroxyl radicals [13]. The degradation rate of each compound was not in agreement with the rate constant values which can be concluded as the hydroxyl radical reaction was not the only predominant degradation route.

Similar comparison studies for the photocatalytic performances of these compounds were conducted by some researchers. Coleman et al. [28] investigated silver and platinum metals on the photocatalytic degradation of several EDCs including bisphenol A and 2,4-dichlorophenol Degussa P25. The degradation efficiencies of BPA and DCP were found similar over TiO_2 under UV-A light irradiation. Kim et al. [29] compared the degradation efficiencies of BPA and pharmaceutically active chemicals – cefaclor, diclofenac, and ibuprofen – over a homogenous catalysis. In contrast to present data, they found that hydrophobic BPA was eliminated more slowly by adsorption over hydrophobic catalysis than diclofenac and ibuprofen. On the other hand, in the presence of H_2O_2, they found the degradability of BPA more favorable than IBU. They stated that the electrical charge of each chemical was the main important factor while hydrophilicity of the compounds was found as the next effective factor.

3.2.1. pH effect

As the solution pH influences the surface charge of the semiconductor, the degradation of DCP, BPA, IBU and FLU at acidic (pH 3.0) and basic (pH 10.0) conditions were investigated and compared with pH 6.5 (Fig. 12).

It can be seen that until its natural pH, the BPA removal increased with an increase in the initial pH and then decreased at basic medium after 4 h: 74.6% (pH = 3.0), 97.7% (pH = 6.5), and 50.0% (pH = 10.0). The order of degradation rates follows pH 6.5 > pH 3.0 > pH 10.0. Wang-2010 reported that the observed trend could be due to the two main factors namely, the adsorption mechanism of BPA on the catalyst surface and the formation of hydroxyl radicals. BPA molecules possess two negative oxygen atoms at the hydroxyl groups and four negative carbon atoms ortho to the phenolic groups [30]. Additionally, the pK_{a1} and pK_{a2} values of BPA are approximately 9.6 and 10.2, respectively. On the other hand, the PZC of $8B-TiO_2$ catalyst was found to be at pH 6.8. Hence, catalyst surface carries positive charge below pH_{pzc} and negatively charged above pH_{pzc}. When pH was raised to >10, deprotonation of BPA into BPA$^-$ and BPA^{2-} increased and the negatively charged surface of $8B-TiO_2$ repelled BPA at pH > 6.8. Similar phenomenon was also observed for DCP degradation over $8B-TiO_2$ catalyst. The DCP degradation—after 5 h– increased from 67.5% at pH = 3.0 to 75.1% at pH = 6.5, and then decreased to 43.9% at pH = 10.0. The pK_a
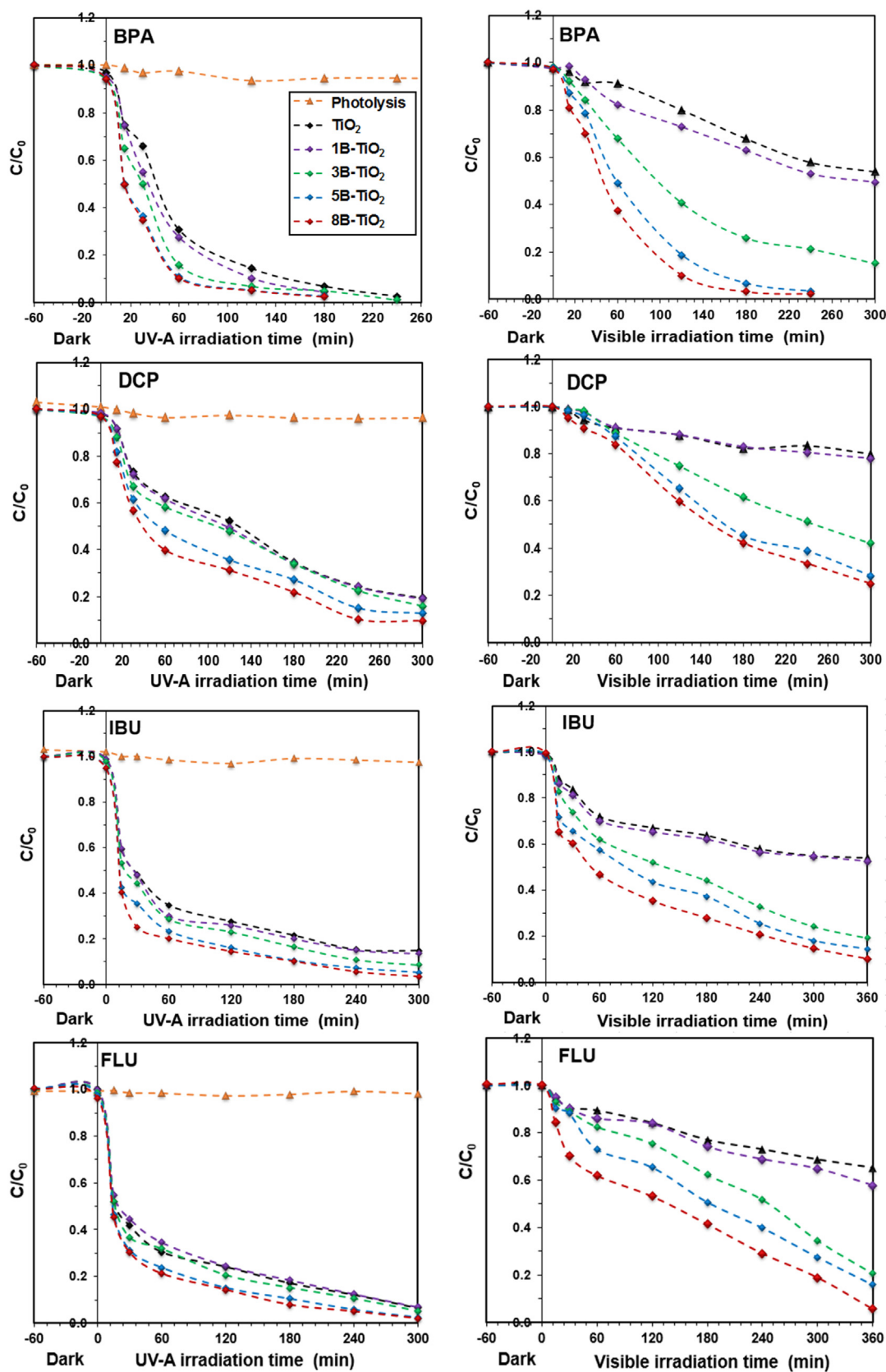
Fig. 11. Comparison of the photocatalytic activities of TiO_2 and $B-TiO_2$ catalysts for the selected pollutants under UV-A and visible light irradiation [pH = 6.5, T = 25–30 °C, C_0 = 20 mg L^{-1}, Catalyst dosage = 1 g L^{-1}, Q_{air} = 2 L min^{-1}].
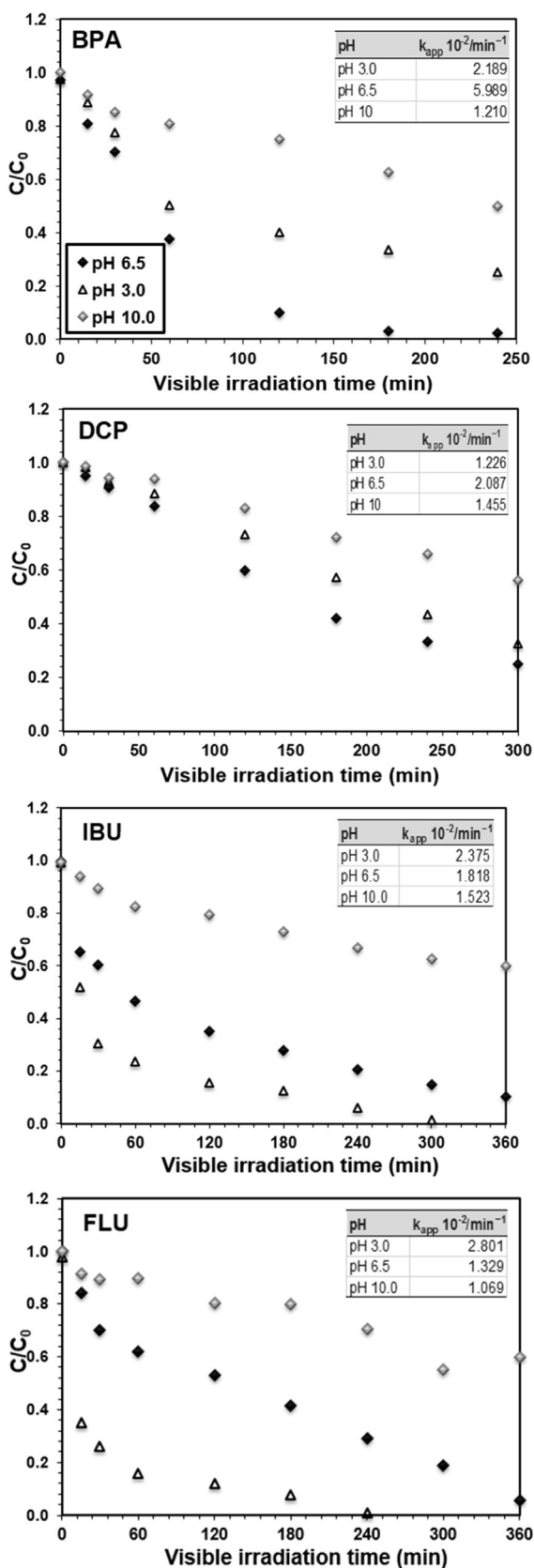
Fig. 12. Influence of pH value on the degradation of target compounds [$C_0 = 20$ mg L^{-1}, Catalyst dosage = 1 g L^{-1}, $Q_{air} = 2$ L min^{-1}].

value of 2,4-DCP is 7.85 ($C_6H_3Cl_2OH \rightarrow C_6H_3Cl_2O^- + H^+$, p$K_a = 7.89$) [7]. When the solution pH is 6.0–6.5 (original pH of DCP), favorable adsorption/degradation occurred between the partially ionized DCP molecules and positively charged surface, where at higher pHs (>pK_a) it decreased owing to the negatively charged $C_6H_3Cl_2O^-$ ions.

As illustrated in Fig. 12, the pH levels played a significant role in IBU and FLU degradation where the reaction was more favorable under acidic conditions than under neutral or alkaline conditions. The best performance was gained at pH 3.0 with 93.8% and 98.2% removal efficiency—after 4 h– for IBU and FLU, respectively. Besides, alkaline and neutral pH values showed poor performance in the IBU (33% at pH 10.0; 79% at pH 6.5) and FLU (29% at pH 10.0; 71% at pH 6.5) degradation. IBU (p$K_a = 4.52$–4.9) and FLU (p$K_a = 4.2$–4.27) are weak acids while the PZC of 8B-TiO$_2$ is 6.8. In alkaline media (pH 10.0), IBU and FLU are electronegative due to ionization and repulsion forces occur between electronegative and deprotonated 8B-TiO$_2$ surface. When pH was above 4.2–4.9, namely 6.5, IBU and FLU were negatively charged, while 8B-TiO$_2$ surface was nearly neutral. In this state, charge neutralization might take place as a removal mechanism, resulting in a higher efficiency when compared with pH 10.0. In acidic medium (pH 3.0), IBU and FLU are electrically neutral and exist in molecular form, while 8B-TiO$_2$ is electropositive. The unionized FLU and IBU molecules might be more easily precipitated and this could facilitate the adsorption of FLU and IBU to the surface of the catalyst.

On the other hand, at their optimum pH values, the average time needed to reach 98% removal of the pharmaceutically active compounds (IBU and FLU) removal was around 4 h which was similar with the degradation time of EDCs. Moreover, about 77% (BPA), 37.4% (DCP) and 60–63% (for IBU and FLU) of organic carbon were completely mineralized after 4 h irradiation, indicating that mineralization takes place quite quickly along with DCP and BPA degradation (Fig. 13(a)). The remaining 30–40% carbon can be attributed to the formation of intermediate byproducts while about 60% intermediates of DCP were produced after degradation.

According to the obtained results, further H_2O_2 effect and cycle experiments for IBU and FLU were conducted at optimum pH 3.0.

3.2.2. Photocatalytic performance of 8B-TiO$_2$ in spiked tap water

As tap water includes various types of salts, organic matter, it is more complex water matrix than deionized water. Therefore, tap water samples spiked with each pollutant (C_0: 3 mg/L) were subjected to degradation tests in order to examine the effect of water matrix. The photocatalyst (8B-TiO$_2$) loading was 0.5 g/L. The tap water composition was as follows: pH 7.39; conductivity 210 µS/cm; TDS 357 mg/L; TOC 3.0 mg/L; SO$_4^{2-}$ 27 mg/L; alkalinity 217 mg CaCO$_3$/L; Cl$^-$ 81 mg/L; NO$_3^-$ 2.8 mg/L; Ca 72.3 mg/L; Mg 16 mg/L; K 5.3 mg/L; Si 4.9 mg/L; Al 0.095 mg/L; Na 52.6 mg/L; Fe 0.009 mg/L.

As shown in Fig. 13(b), BPA could be degraded within 90 min in distilled water while slightly slow degradation was observed in tap water. Similarly, about 95% degradation of IBU and FLU in distilled water was achieved in 90 min, while at the same reaction time around 85% degradation was achieved in the tap water. The reduction in the degradation efficiency in tap water is mainly attributed to the interfering anions (i.e., sulfate and phosphate) present in tap water which scavenge the radical species or absorb the UV radiation.

3.2.3. H_2O_2 effect

Hydrogen peroxide (H_2O_2) is one of the most powerful oxidants generating HO$^\bullet$ (HO$^\bullet$/H$_2$O; E = 1.8–2.7 V) via its decomposition [2]. One molecule of hydrogen peroxide leads to the generation of two HO$^\cdot$ radicals through the absorption of light ($H_2O_2 + h\nu \rightarrow 2HO^\bullet$). The effect of H_2O_2 on the degradation of the target pollutants
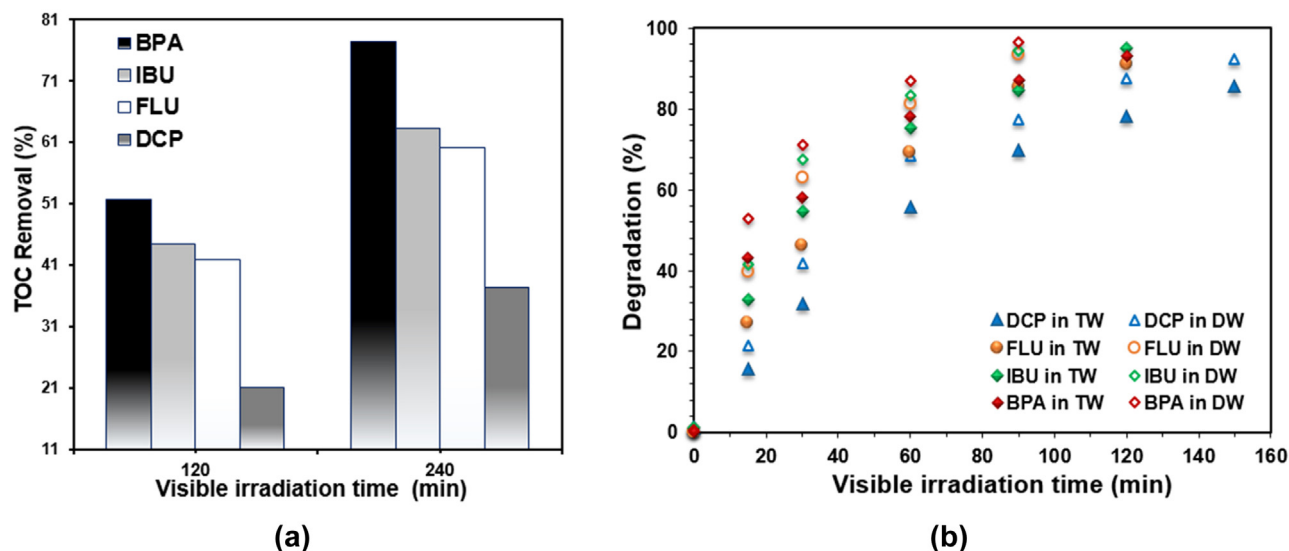
Fig. 13. (a) TOC conversion ratios after 120 and 240 min visible illumination over 8B-TiO$_2$ catalyst (b) Degradation in tap water and distilled water [C$_0$ = 3 mg L^{-1}, Catalyst dosage = 0.5 g L^{-1}, Q$_{air}$ = 2 L min^{-1}].
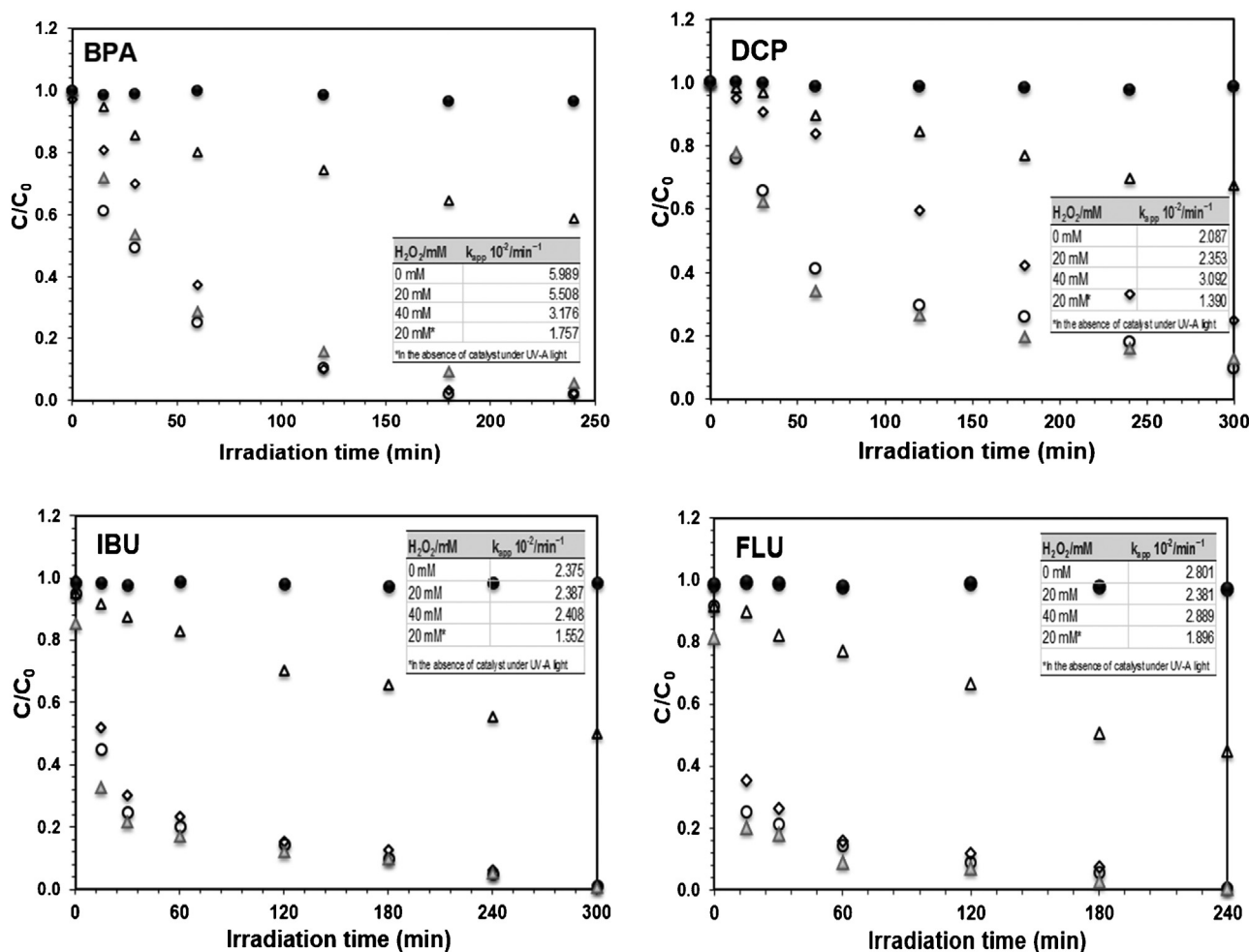
Fig. 14. Degradation of EDCs and NSAIDs in the presence of H$_2$O$_2$: (△) UV-A/H$_2$O$_2$ (20 mM), (●)Visible light/H$_2$O$_2$ (20 mM), (◊) 8B-TiO$_2$/Visible light (○) 8B-TiO$_2$/Visible light/H$_2$O$_2$ (20 mM), (▲) 8B-TiO$_2$/Visible light/H$_2$O$_2$ (40 mM).

under visible irradiation was studied with H$_2$O$_2$ concentrations of 20 mM and 40 mM and the results are illustrated in Fig. 14. In order to confirm the enhancement effect of H$_2$O$_2$ with B-doped catalyst, solutions were irradiated under UV-A/H$_2$O$_2$ and Visible light/H$_2$O$_2$ systems. As expected, no degradation occurred under Visible light/H$_2$O$_2$ system and approximately 30% of selected com-
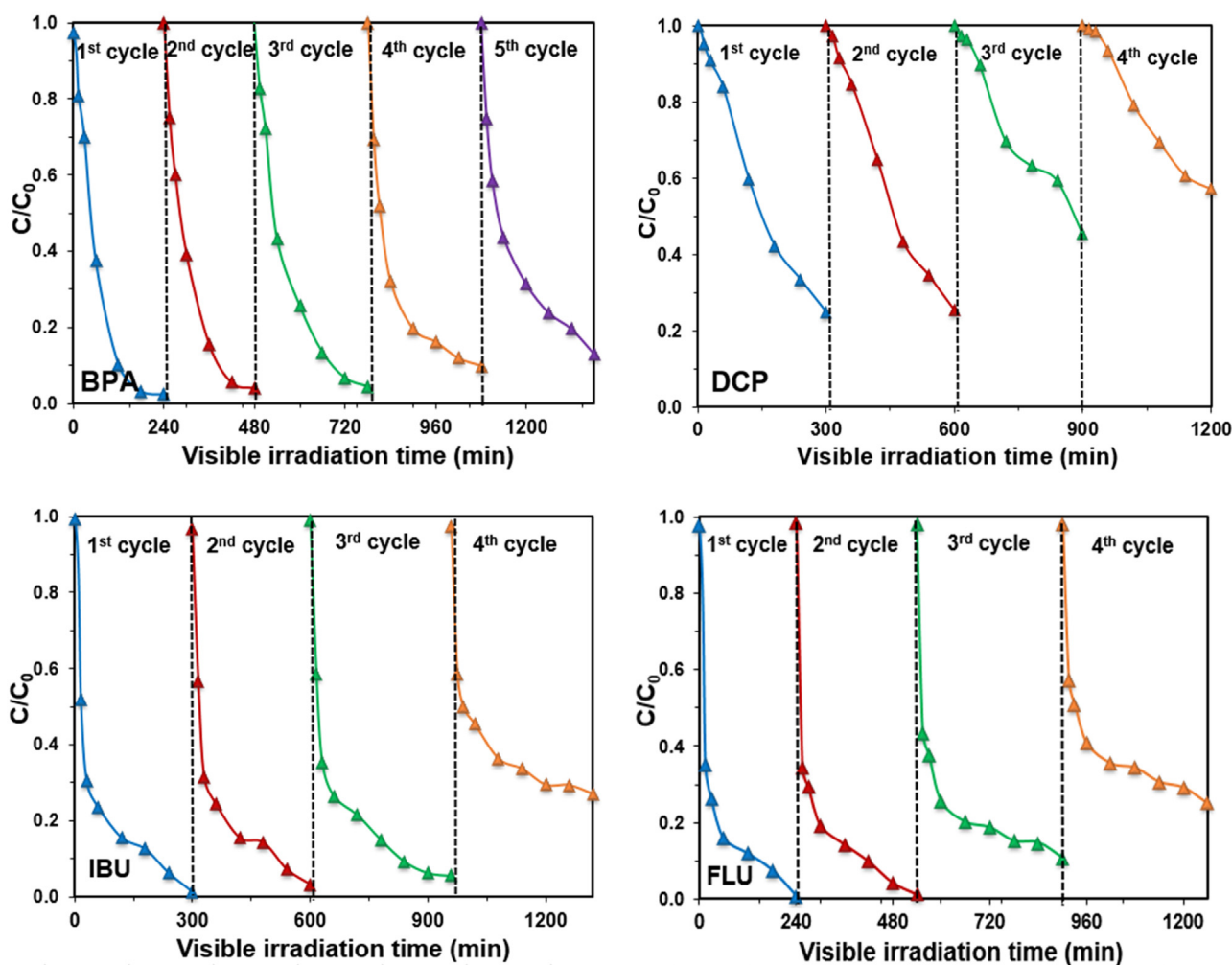
Fig. 15. Cycling degradation curves of the selected EDCs and NSAIDs.

pounds were degraded under UV-A/H_2O_2 system. In the presence of the B-doped catalyst, with an increase in the H_2O_2 concentration from 0 to 20 mM, within 60 min, the DCP and BPA degradation increased from 16% to 58% and 62% to 74%, respectively. Similarly, IBU and FLU removals increased from 76% to 79% and 84% to 86%, respectively. It was observed that the bisphenol A and dichlorophenol removal increased significantly in the presence of H_2O_2. On the other hand, ibuprofen and flurbiprofen degradation were not noticeably enhanced reflecting that EDCs oxidation was relatively easier. Under visible irradiation the H_2O_2 decomposition can be explained via the interaction between H_2O_2 and TiO_2 which forms surface complex ($\equiv Ti^{IV}-OOH$) and extends the photoresponse of TiO_2 resulting the system absorb visible light [31,32]. Moreover, further increase in the H_2O_2 concentration (40 mM) has a slight effect on the BPA degradation owing to the self-scavenging effect of $HO^\bullet$ radicals [2].

3.2.4. Photocatalyst stability

In order to evaluate the catalytic stability and reusability of 8B-TiO_2 catalyst, four or five recycling tests for the target pollutants have been performed under visible light irradiation. After each cycle, the catalyst was collected by centrifugation, washed with distilled water and dried in the oven 100 °C for 3 h before reused. As shown in Fig. 15, 75% of DCP was degraded at the first cycle while it decreased significantly to 42% at the fifth cycle. For IBU and FLU degradation, the catalyst performance decreased significantly after

being used repetitively for 4 times. The reduced catalysis ability for the target compounds could be explained by the tiny loss of the photocatalyst.

On the other hand, BPA degradation curves were found very close to each other and reaches 86.9% after five recycling runs, indicating that 8B-TiO_2 photocatalyst is stable for effective BPA degradation under visible light irradiation. In order to examine the effect of boron content in the BPA degradation tests, boron concentrations were analyzed in the aliquots at time intervals (30 min, 60 min, 120 min, 240 min) for each cycle. The results revealed that no boron was leached after five consecutive runs.

4. Conclusions

B-doped TiO_2 visible light-activated photocatalysts were synthesized by solvothermal method by using tetra-butyl titanate and boric acid. The photocatalytic activity of as-prepared B-doped TiO_2 catalysts were determined by degradation of endocrine disruptors, DCP, BPA and pharmaceutically active chemicals, IBU and FLU under visible light. The incorporation of boron improved the photocatalytic activity of TiO_2 under visible light illumination mainly which is likely due to the decreased band gap energy and more developed surface area. Based on the reusability tests, 8B-TiO_2 catalyst exhibited stability for BPA degradation.

Acknowledgments

Appendix A. Supplementary data

Supplementary data associated with this article can be found, in the online version, at http://dx.doi.org/10.1016/j.apcatb.2016.07.016.

References

[1] P. Westerhoff, Y. Yoon, S. Snyder, A.E. Wert, Environ. Sci. Technol. 39 (2005) 6649–6663.
[2] J. Sharma, I.M. Mishra, V. Kumar, J. Environ. Manage. 156 (2015) 266–275.
[3] A.M.F. Orozco, E.M. Contreras, N.E. Zaritzky, Int. Biodeterior. Biodegrad. 106 (2016) 1–9.
[4] V. Maroga Mboula, V. Héquet, Y. Andrés, L.M. Pastrana-Martínez, J.M. Donà-Rodríguez, A.M.T. Silva, P. Falaras, Water Res. 47 (2013) 3997–4005.
[5] J. Sin, S. Lam, K. Lee, A.R. Mohamed, J. Colloid Interface Sci. 401 (2013) 40–49.
[6] S. Barışçı, F. Ulu, M. Sillanpää, A. Dimoglo, Chem. Eng. J. 262 (2015) 1218–1225.
[7] M. Chang, Y. Hsieh, T. Cheng, K. Yao, M. Wei, C. Chang, Thin Solid Films 517 (2009) 3888–3891.
[8] R. Khan, S. Woo, T. Kim, C. Nam, Mater. Chem. Phys. 112 (2008) 167–172.
[9] C. Chang, Y. Fu, M. Hu, C. Wang, G. Shan, L. Zhu, Appl. Catal. B 143 (2013) 553–560.
[10] G. Dai, S. Liu, Y. Liang, J. Alloys Compd. 608 (2014) 44–48.
[11] Q. Wang, H. Jiang, S. Zang, J. Li, Q. Wang, J. Alloys Compd. 586 (2014) 411–419.
[12] Y. Wu, M. Xing, J. Zhang, J. Hazard, Materials 192 (2011) 368–373.
[13] D.H. Quińones, A. Rey, P.M. Álvarez, F.J. Beltrán, G. Li Puma, Appl. Catal. B 178 (2015) 74–81.
[14] X. Lan, L. Wang, B. Zhang, B. Tian, J. Zhang, Catal. Today 224 (2014) 163–170.
[15] L. Liang, Y. Yulin, L. Xinrong, F. Ruiqing, S. Yan, L. Shuo, et al., Appl. Surf. Sci. 265 (2013) 36–40.
[16] A. Zaleska, E. Grabowska, J.W. Sobczak, M. Gazda, J. Hupka, Appl. Catal. B 89 (2009) 469–475.
[17] J. Zheng, Z. Liu, X. Liu, X. Yan, D. Li, W. Chu, J. Alloys Compd. 509 (2011) 3771–3776.
[18] R.P. Cavalcante, R.F. Dantas, B. Bayarri, O. González, J. Giménez, S. Esplugas, A.M. Junior, Catal. Today 2 (2014) 28–31.
[19] F. Helfferich, Ion Exchange, Dover, New York, N.Y, 1995.
[20] X. Bai, X. Zhang, Z. Hua, W. Ma, Z. Dai, X. Huang, et al., J. Alloys Compd. 599 (2014) 10–18.
[21] X. Xue, Y. Wang, H. Yang, Appl. Surf. Sci. 264 (2013) 94–99.
[22] D. Peak, G.W. Luther, D.L. Sparks, Geochim. Cosmochim. Acta 67 (2003) 2551–2560.
[23] D. Chen, D. Yang, Q. Wang, Z. Jiang, Ind. Eng. Chem. Res. (2006) 4110–4116.
[24] X. Lu, B. Tian, F. Chen, J. Zhang, Thin Solid Films 519 (2010) 111–116.
[25] L. Artiglia, D. Lazzari, S. Agnoli, G.A. Rizzi, G. Granozzi, J. Phys. Chem. C 117 (2013) 13163–13172.
[26] I. Dobrosz-Gómez, M.A. Gómez-García, S.M. López Zamora, E. GilPavas, J. Bojarska, M. Kozanecki, J.M. Rynkowski, C. R. Chim. 18 (2015) 1170–1182.
[27] Y. Fu, C. Chang, P. Chen, X. Chu, L. Zhu, J. Hazard. Mater. 254–255 (2013) 185–192.
[28] H.M. Coleman, K. Chiang, R. Amal, Chem. Eng. J. 113 (2005) 65–72.
[29] J. Kim, S. Kim, C. Lee, H. Kwon, Ind. Eng. Chem. Res. 48 (2009) 1586–1592.
[30] X. Wang, T. Lim, Appl. Catal. B 100 (2010) 355–364.
[31] W. Liu, H. Liu, Z. Ai, J. Hazard. Mater. 288 (2015) 97–103.
[32] X. Li, C. Chen, J. Zhao, Langmuir 17 (2001) 4118–4122.